

THE $\log N - \log S$ AND THE BROADBAND PROPERTIES OF THE SOURCES IN THE HELLAS2XMM SURVEY

A. Baldi¹, S. Molendi¹, A. Comastri², F. Fiore³, G. Matt⁴, and C. Vignali⁵

¹Istituto di Fisica Cosmica - CNR, via Bassini 15, I-20133 Milano, Italy

²Osservatorio Astronomico di Bologna, via Ranzani 1, I-40127 Bologna, Italy

³Osservatorio Astronomico di Roma, via Frascati 33, I-00040 Monteporzio, Italy

⁴Dipartimento di Fisica - Università di Roma Tre, via della Vasca Navale 84, I-00146 Roma, Italy

⁵Dept. of Astronomy and Astrophysics - The Pennsylvania State University, 525 Davey Lab, University Park, PA 16802 USA

ABSTRACT

We present the first results from an *XMM-Newton* serendipitous medium-deep survey, which covers nearly three square degrees. We show the $\log N - \log S$ distributions for the 0.5-2, 2-10 and 5-10 keV bands, which are found to be in good agreement with previous determinations and with the predictions of XRB models. In the soft band we detect a break at fluxes around 5×10^{-15} cgs. In the harder bands, we fill in the gap at intermediate fluxes between deeper *Chandra* and *XMM-Newton* observations and shallower *BeppoSAX* and *ASCA* surveys. Moreover, we present an analysis of the broad-band properties of the sources.

Key words: galaxies: active — X-rays: diffuse background — X-rays: galaxies

1. INTRODUCTION

While in the soft band (0.5-2 keV) *ROSAT* (Hasinger et al. 1998) and especially *Chandra* (Rosati et al. 2001) has resolved almost all the XRB, in the hard band (2-10 keV) the XRB has been resolved at a 25%-30% level with *BeppoSAX* and *ASCA* surveys (Cagnoni et al. 1998; Giommi et al. 2000) and recently at a 90% with *Chandra* (Rosati et al. 2001). Moreover, in the very hard band (5-10 keV) the fraction resolved by *BeppoSAX* is around 30% (Fiore et al. 1998) and recently in the *XMM-Newton* Lockman Hole deep pointing a 60% is reached (Hasinger et al. 2001). The optical counterparts of the objects making the XRB are predominantly Active Galactic Nuclei (AGN). In the soft band the predominant fraction is made by unabsorbed AGN, with a small fraction of absorbed AGN (Schmidt et al. 1998). The fraction of absorbed type-2 AGN rises if we consider the spectroscopic identifications of hard X-ray sources in *BeppoSAX*, *ASCA* and *Chandra* surveys (Fiore et al. 2001; Della Ceca et al. 2000; Tozzi et al. 2001).

The X-ray and optical observations are consistent with current XRB synthesis models (Comastri et al. 1995; Gilli et al. 2001), which explain the hard XRB spectrum with an appropriate mixture of absorbed and unabsorbed AGN, by introducing the corresponding luminosity function and cosmological evolution. However, these models require the

presence of a significant population of type-2 QSOs (Norman et al. 2001), not yet detected in sufficient quantities. Type-2 QSOs are rare (so far, only a few are known), luminous and hard (heavily absorbed in the soft band). A good way of finding them is to perform surveys in the hard X-ray bands, covering large solid angles. The large throughput and effective area, particularly in the harder bands, make *XMM-Newton* currently the best satellite to perform hard X-ray surveys.

In this poster contribution we present results from the HELLAS2XMM survey (Baldi et al. 2002), one of its main goals is to constrain the contribution of absorbed AGN to the XRB.

2. DATA PREPARATION AND CLEANING

We use the XMM-SAS analysis software tasks *epproc* and *emproc* to linearize the event files. Before processing, datasets are corrected for the attitude of the satellite in order to have absolute positions in the sky. The Attitude History File(AHF) coordinates are given to the SAS task *odf fix* which performs the correction.

The event files produced by *epproc* and *emproc* are cleaned from:

- hot pixels; with a procedure (developed at IFC/CNR-Milan by A. De Luca) which uses cosmic ray IRAF tasks to localize the pixels to be rejected in each CCD and XMM-SAS task *evselect* for removing them from the event files;
- soft proton flares; analysing the light curves at energies greater than 10keV and setting a threshold for good time intervals of 0.15 cts/s for MOS units and of 0.35 cts/s for pn unit.

A complete set of MOS1, MOS2 and pn 600x600 pixel images (1 pixel = 4.35 arcsec) is generated using XMM-SAS task *evselect* in the 0.5-2, 2-10, 2-4.5, 4.5-10 and 0.5-10 keV bands. MOS and pn images are merged together in order to increase the signal-to-noise ratio of the sources and go deeper.

A corresponding set of exposure maps is generated to account for spatial quantum efficiency, mirror vignetting and field of view of each instrument, running XMM-SAS task *eexppmap*. The so-created exposure maps are not completely satisfactory, since the evaluation of quantum efficiency, filter transmission, and vignetting is performed

assuming an event energy which corresponds to the mean of the energy boundaries. In the 2-10 keV band, this may lead to inaccuracies in the estimate of these key quantities, thus we create the 2-10 keV band exposure map as a weighted mean of the 2-4.5 keV and the 4.5-10 keV exposure maps (assuming an underlying power-law spectral model with $\Gamma = 1.7$).

XMM-SAS task *esplinemap* creates a background map by

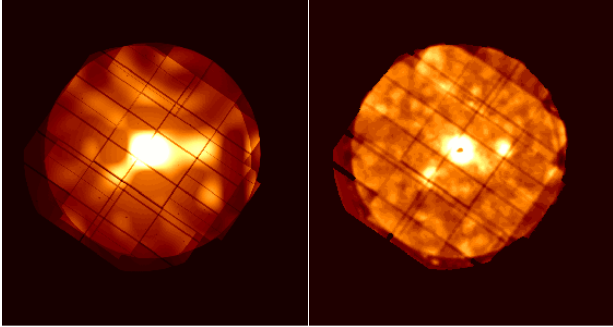


Figure 1. Left: XMM-SAS standard background map. Right: corrected background map.

removing all the sources above a fixed maximum likelihood threshold and fitting the remaining with a cubic spline. Even using the maximum number of spline nodes (20), the fit is not enough flexible to take into account the local variations of the background. We correct the background map produced by XMM-SAS, pixel by pixel, comparing the mean value in it with that of the so-called cheesed image, within a radius of $3 \cdot r_{0.68}$ ($r_{0.68}$ = radius corresponding to an encircled energy fraction (EEF) of 0.68). A comparison between XMM-SAS standard background map and our corrected map is shown in Figure 1.

3. SOURCE DETECTION AND CHARACTERIZATION

A preliminary detection run, using XMM-SAS *ebordetect*, is performed in each energy band, in order to create a list of candidate sources. Each source is characterized using a radius corresponding to an EEF of $\alpha=0.68$.

The source counts S and their error σ_S are determined as

$$S = \frac{cts_{src} - cts_{bkg}}{\alpha}$$

$$\sigma_S = \frac{1 + \sqrt{cts_{src} + 0.75}}{\alpha}$$

The countrate is $cr = \frac{S}{T_{tot}}$ where T_{tot} is the sum of MOS1, MOS2 and pn exposure times. The corresponding flux is $F_x = cf \cdot cr$ where cf is calculated from the

$$\frac{T_{tot}}{cf} = \frac{T_{MOS1}}{cf_{MOS1}} + \frac{T_{MOS2}}{cf_{MOS2}} + \frac{T_{pn}}{cf_{pn}}$$

Moreover we compute p , the poissonian probability that counts originate from a background fluctuation, from the

$$\sum_{n=cts_{src}}^{\infty} e^{-cts_{bkg}} \frac{cts_{bkg}^n}{n!} > p$$

and choose a threshold of $p = 2 \times 10^{-4}$ to decide whether to accept or not a detected source.

4. THE SURVEY

The HELLAS2XMM survey (Baldi et al. 2002) currently uses the 15 *XMM-Newton* calibration and performance verification phase fields shown in table 1. All the fields are at high galactic latitude ($|b_{II}| > 27^\circ$), have low galactic N_H (a few 10^{20} cm^{-2}) and at least 15 ksec of good observing time. The sky coverage of the sample has been

Table 1. The HELLAS2XMM survey sample.

Target	$N_H \text{ (cm}^{-2}\text{)}$	$b_{II} (^\circ)$
PKS0537-286	$2.1 \cdot 10^{20}$	-27.3
PKS0312-770	$8 \cdot 10^{20}$	-37.6
MS0737.9+7441	$3.5 \cdot 10^{20}$	29.6
Lockman Hole	$5.6 \cdot 10^{19}$	53.1
Mkn 205	$3 \cdot 10^{20}$	41.7
BPM 16274	$3.2 \cdot 10^{20}$	-65.0
MS1229.2+6430	$2 \cdot 10^{20}$	52.8
PKS0558-504	$4.5 \cdot 10^{20}$	-28.6
Mkn 421	$7 \cdot 10^{19}$	65.0
Abell 2690	$1.9 \cdot 10^{20}$	-78.4
G158-100	$2.5 \cdot 10^{20}$	-74.5
GD153	$2.4 \cdot 10^{20}$	84.7
IRAS13349+2438	$1.2 \cdot 10^{20}$	60.6
Abell 1835	$2.3 \cdot 10^{20}$	60.6
Mkn 509	$4.1 \cdot 10^{20}$	-29.9

computed using the exposure maps of each instrument, the background map of the merged image and a model for the PSF. We adopt the off-axis angle dependent PSF model implemented in *XMM-SAS ebordetect* task.

At each image pixel (x, y) we evaluate, within a radius $r_{0.68}$, the total background counts (from the background map). From these we calculate the minimum total counts (source + background) necessary for a source to be detected at a probability $p = 2 \times 10^{-4}$ (defined in Section 3). The mean exposure times for *MOS1*, *MOS2* and *pn*, evaluated from the exposure maps within $r_{0.68}$, are used to compute the count rate cr . From the count rate-to-flux conversion factor cf (computed as in Section 3) we build a flux limit map and straightforwardly calculate the sky coverage of a single field.

Summing the contribution from all fields we obtain the

total sky coverage of the survey, which is plotted in Figure 2, in three different energy bands.

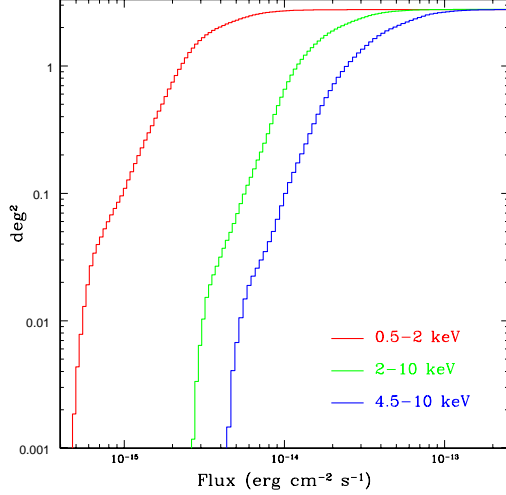


Figure 2. The total sky coverage of the survey in the 0.5–2 keV (red), 2–10 keV (green) and 4.5–10 keV band (blue).

5. THE $\log N - \log S$ RELATION

The $\log N - \log S$ distributions are plotted in Figure 3 and contain 1022, 495 and 100 sources, for the 0.5–2 keV, 2–10 keV and 5–10 keV band, respectively.

In the 0.5–2 keV band the distribution shows a flattening around $5 \times 10^{-15} \text{ erg cm}^{-2} \text{ s}^{-1}$, similarly to *ROSAT* data (Hasinger et al. 1998) although with a flatter differential slope index at faint fluxes. We are also in good agreement with *Chandra* Deep Field South data (Giacconi et al. 2001). In the 2–10 keV band we find that the distribution is significantly sub-euclidean, in contrast to *BeppoSAX* and *ASCA* findings (Giommi et al. 2000; Cagnoni et al. 1998; Ueda et al. 1999), indicating that the $\log N - \log S$ flattens at fainter fluxes. Anyhow it represents a link between *Chandra* (Giacconi et al. 2001) and *BeppoSAX*-*ASCA* observation, sampling an intermediate flux range. The 5–10 keV $\log N - \log S$ is consistent with an euclidean slope and samples an intermediate flux range between *XMM-Newton* deeper observations (Hasinger et al. 2001) and *BeppoSAX* shallower *HELLAS* survey (Fiore et al. 1998).

6. HARDNESS RATIO ANALYSIS

We divided the sample of sources detected both in 0.5–2 keV band and in 2–4.5 keV band in two subsamples containing the brighter ($F_{0.5-2\text{keV}} > 2 \times 10^{-14} \text{ erg cm}^{-2} \text{ s}^{-1}$) and the fainter ($F_{0.5-2\text{keV}} \leq 2 \times 10^{-14} \text{ erg cm}^{-2} \text{ s}^{-1}$) sources, respectively and we compute for them the

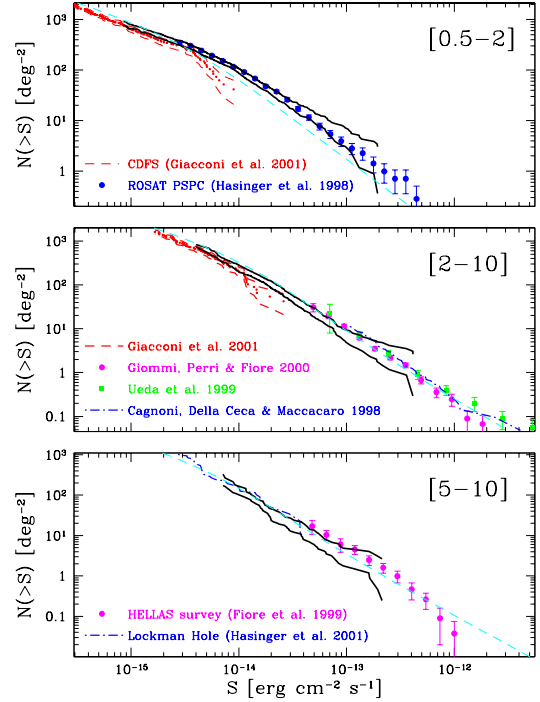


Figure 3. The cumulative $\log N - \log S$ in the 0.5–2 keV (top), 2–10 keV (center) and 5–10 keV band (bottom). In all diagrams the black thick solid lines are the upper and lower limits of our $\log(N)$ - $\log(S)$. The dashed cyan lines are the predictions of the XRB synthesis models from Comastri et al.(2001).

hardness ratio:

$$HR_1 = \frac{cr_{2-4.5} - cr_{0.5-2}}{cr_{2-4.5} + cr_{0.5-2}}$$

As shown in Figure 4 and in Table 2, the faint sample

Table 2. HR_1 distribution for the faint and the bright sample.

	$N(HR_1 < -0.35)$	$N(HR_1 \geq -0.35)$
Faint sample	654	84
Bright sample	107	0

shows a tail of hard sources which is not present in the bright sample. The probability of having 84 sources with $HR_1 \geq -0.35$ in the faint sample and no sources with $HR_1 \geq -0.35$ in the bright sample is $\sim 10^{-6}$, so the progressive hardening of the sources towards fainter fluxes seems to be highly significant.

A further analysis of the hardness ratio has been carried out on the 4.5–10 keV sample. In Figure 5 the relation

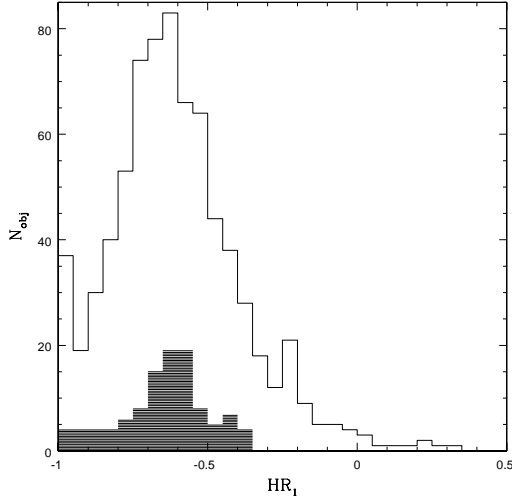


Figure 4. The distribution of hardness ratio HR_1 . Void histogram: sources with $F_{0.5-2\text{keV}} \leq 2 \times 10^{-14} \text{ erg cm}^{-2} \text{ s}^{-1}$. Shaded histogram: sources with $F_{0.5-2\text{keV}} > 2 \times 10^{-14} \text{ erg cm}^{-2} \text{ s}^{-1}$.

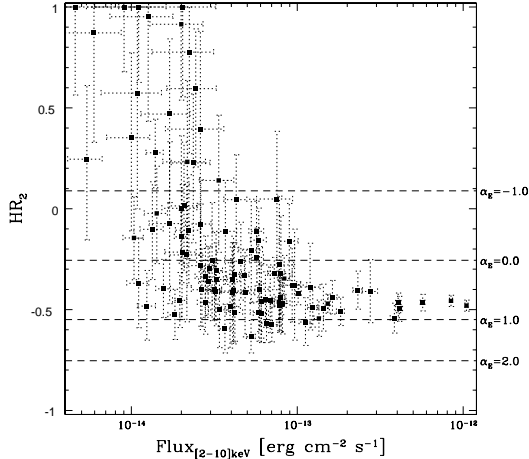


Figure 5. 2-10 keV flux vs. HR_2 for the sources detected in the 4.5-10 keV band. The dashed lines indicate the hardness ratios of the sources according to a power-law model (galactic absorption) with spectral index α_E .

between the 2-10 keV flux and the hardness ratio

$$HR_2 = \frac{cr_{4.5-10} - cr_{2-4.5}}{cr_{4.5-10} + cr_{2-4.5}}$$

for sources detected in the 4.5-10 keV band is plotted. The diagram shows a progressive hardening of the sources when going towards fainter fluxes. While the lack of sources in the bottom left of the figure is due to a selection effect (because we are more sensitive in the 2-4.5 keV than in the 4.5-10 keV band), there is no apparent reason for having no hard sources at fluxes greater than a few 10^{-14} erg

$\text{cm}^{-2} \text{ s}^{-1}$.

The population of harder sources we detect, probably consists of AGN having substantial absorbing column densities ($N_H > 10^{22} \text{ cm}^{-2}$).

7. SUMMARY

We are carrying out a serendipitous *XMM-Newton* survey. We currently cover nearly three square degrees in 15 fields observed during satellite calibration and performance verification phase. This is, to date, the *XMM-Newton* survey with the largest solid angle.

The main results can be summarized as follows:

- The $\log N$ - $\log S$ relations in the 0.5-2 keV, 2-10 keV and 5-10 keV band are in agreement with previous determinations;
- in the hard bands we sample an intermediate flux range: deeper than *ASCA* and *BeppoSAX* and shallower than *Chandra* and *XMM-Newton* deep surveys
- We find an evidence for hard sources emerging below 0.5-2 keV fluxes of $2 \times 10^{-14} \text{ erg cm}^{-2} \text{ s}^{-1}$ and 2-10 keV fluxes of $10^{-13} \text{ erg cm}^{-2} \text{ s}^{-1}$.

ACKNOWLEDGEMENTS

We thank A. De Luca for developing the hot pixel cleaning algorithm. We are also grateful to G. Zamorani, G. C. Perola and all members of the HELLAS2XMM team for useful discussions. AB and SM acknowledge partial financial support by ASI I/R/190/00 contract.

REFERENCES

- Baldi A., Molendi S., Comastri A., Fiore F., Matt G., Vignali C. 2002, *ApJ* 564, 190
- Cagnoni I., Della Ceca R., Maccacaro, T. 1998, *ApJ* 493, 54
- Comastri A., Setti G., Zamorani G., Hasinger G. 1995, *A&A* 296, 1
- Comastri A., Fiore F., Vignali C., Matt G., Perola G.C., La Franca F. 2001, *MNRAS* 327, 781
- Della Ceca R., Maccacaro T., Rosati P., Braito V. 2000, *A&A* 355, 121
- Fiore F., La Franca F., Giommi P., Elvis M., Matt G., Comastri A., Molendi S., Gioia I. 1999, *MNRAS* 306, L55
- Fiore F., Comastri A., La Franca F., Vignali C., Matt G., Perola G.C. 2001 proceedings of the ESO/ECF/STSCI workshop on "Deep Fields", astro-ph/0102041
- Giacconi R., Rosati P., Tozzi P. et al. 2001, *ApJ* 551, 624
- Gilli R., Salvati M., Hasinger G. 2001, *A&A* 366, 407
- Giommi P., Perri M., Fiore, F. 2000, *A&A* 362, 799
- Hasinger G., Burg R., Giacconi R., Schmidt M., Trümper J., Zamorani, G. 1998, *A&A* 329, 482
- Hasinger G., Altieri B., Arnaud M. et al. 2001, *A&A* 365, L45
- Norman C., Hasinger G., Giacconi R. et al. 2001, *ApJ* accepted, astro-ph/0103198
- Rosati P., Tozzi P., Giacconi R. et al. 2001, *ApJ* accepted, astro-ph/0110452
- Schmidt M., Hasinger G., Gunn J. et al. 1998, *A&A* 329, 495
- Tozzi P., Rosati P., Nonino, M. et al. 2001, *ApJ* 562, 42
- Ueda Y., Takahashi T., Inoue H. et al. 1999, *ApJ* 518, 656